Excited rotational states of molecules in a superfluid

Igor N. Cherepanov,[1] Giacomo Bighin,[1] Constant A. Schouder,[2] Adam S. Chatterley,[2] Simon H. Albrechtsen,[2]
Alberto Viñas Muñoz,[2] Lars Christiansen,[2] Henrik Stapelfeldt [ ],[2,*] and Mikhail Lemeshko[1,†]

[1]*Institute of Science and Technology Austria, Am Campus 1, 3400 Klosterneuburg, Austria*
[2]*Department of Chemistry, Aarhus University, 8000 Aarhus C, Denmark*

We combine experimental and theoretical approaches to explore excited rotational states of molecules embedded in helium nanodroplets using CS_2 and I_2 as examples. Laser-induced nonadiabatic molecular alignment is employed to measure spectral lines for rotational states extending beyond those initially populated at the 0.37 K droplet temperature. We construct a simple quantum-mechanical model, based on a linear rotor coupled to a single-mode bosonic bath, to determine the rotational energy structure in its entirety. The calculated and measured spectral lines are in good agreement. We show that the effect of the surrounding superfluid on molecular rotation can be rationalized by a single quantity, the angular momentum, transferred from the molecule to the droplet.

Perhaps the most intriguing example of quantized rotational motion of molecules in a liquid is that of molecules embedded in nanometer-size droplets of superfluid helium. Infrared absorption spectroscopy of many different molecules has established that the rotational energy structure is similar to that of gas-phase molecules. In particular, for linear molecules the rotational energy E_J can be expressed as [1–3]

$$E_J = B^*J(J+1) - D^*J^2(J+1)^2. \qquad (1)$$

Here J is the rotational angular momentum of the molecule and B^* and D^* are, respectively, the rotational and centrifugal distortion constants, which assume renormalized values compared to their gas-phase counterparts B and D. Theoretical models have been developed to describe renormalization of the spectroscopic constants [2,4–12] and led to the following insights. (i) A molecule corotates with a nonsuperfluid He density component resulting in a larger moment of inertia and hence a smaller rotational constant compared to that of the isolated molecule. (ii) When J increases, the effective He-molecule coupling increases [8], which leads to the J-dependent decrease of the rotational constant $D^*(J+1)$ [cf. (1)], with D^* typically 10^2–10^4 times larger than D [13].

The experimental knowledge of the rotational structure of molecules in He droplets has been obtained almost exclusively from IR spectroscopy. Due to selection rules, IR spectroscopy can only provide information about E_J of those rotational levels that are initially populated (actually one level higher than the highest significantly populated level, due to selection rules $\Delta J = \pm 1$). At a 0.37 K temperature of the droplets, this is the lowest-lying rotational state up to $J \sim 5$ [14–16] depending on B. Consequently, the question of what happens

to E_J when J is increased beyond the values populated at 0.37 K remains unanswered by experiments. Notably, Eq. (1) is not of any use in this regime as it predicts that E_J will start decreasing when J exceeds a rather small value (e.g., $J \sim 10$ for OCS molecules). Furthermore, this question also has not been answered by theory. Here we combine theoretical and experimental studies to get insight into rotationally excited states of molecules in He nanodroplets.

Experimentally, we form rotational wave packets [17,18] in the molecules by a picosecond alignment pulse and measure the resulting time-dependent degree of alignment. Fourier transformation of such traces reveals the energy of the rotational states in the wave packets, a technique established for gas-phase molecules [19–22] and recently demonstrated for He-solvated molecules in the limit of weak alignment pulses [23]. We conduct measurements for several alignment pulse intensities to systematically map out the rotational energy structure and thereby circumvent the selection rule limitations of IR spectroscopy.

The experimental setup is almost the same as that used in [23]. Briefly, helium nanodroplets, doped with at most one CS_2 or I_2 molecule, are irradiated by two linearly polarized laser beams inside a velocity map imaging spectrometer. The 2.3-ps pulses in the alignment beam set the molecules into rotation. Their time-dependent alignment is measured through Coulomb explosion, induced by the 40-fs pulses in the probe beam, and detection of two-dimensional velocity images of S^+ or IHe^+ ions, respectively. Each probe pulse is delayed t with respect to an alignment pulse. From the ion images, the degree of the molecular alignment $\langle \cos^2 \theta_{2D} \rangle$ is determined, θ_{2D} being the angle between the alignment pulse polarization and the projection of the velocity vector of a S^+ or IHe^+ ion on the detector. For details see [24], which includes Refs. [25–27].

The left column in Fig. 1 shows $\langle \cos^2 \theta_{2D} \rangle(t)$ for CS_2 molecules at different fluences of the alignment pulse and

*Corresponding author: henriks@chem.au.dk
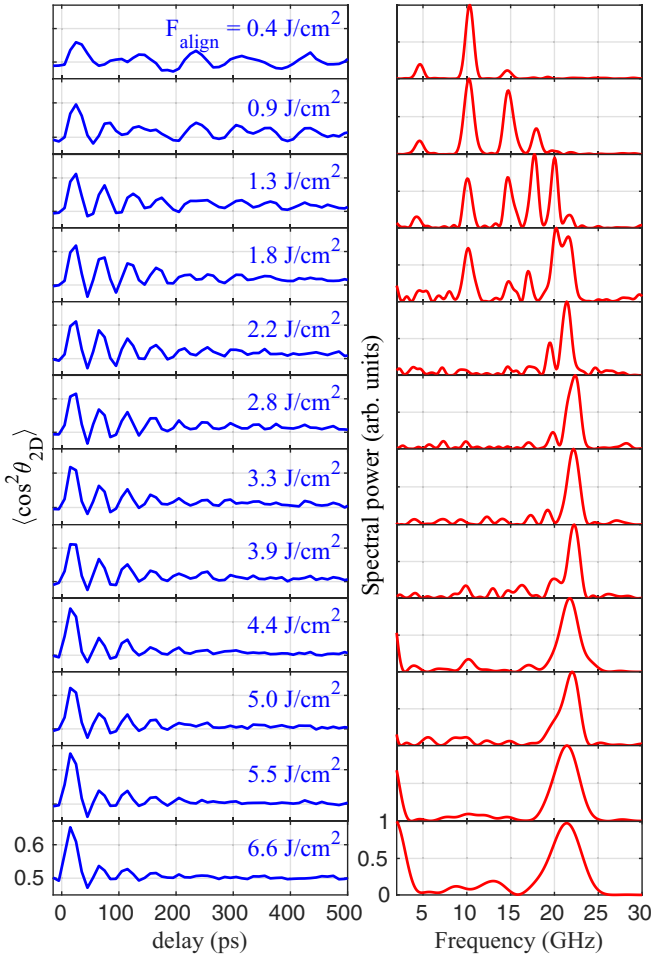†Corresponding author: mikhail.lemeshko@ist.ac.at

FIG. 1. The left column shows $\langle \cos^2 \theta_{2D} \rangle(t)$ for CS$_2$ molecules at 12 different fluences of the alignment pulse given in each panel and the right column shows the power spectra of the corresponding $\langle \cos^2 \theta_{2D} \rangle$ traces.

the right column shows the corresponding power spectra obtained by Fourier transformation of the $\langle \cos^2 \theta_{2D} \rangle$ traces.[1] Although the results for I$_2$ are qualitatively similar, the CS$_2$ spectra are easier to visually interpret due to the absence of odd rotational states. At the lowest fluences, clearly separated peaks in the spectra are observed. When the fluence F is increased, the spectrum shifts to higher frequencies, consistent with the expectation that a stronger pulse adds more rotational angular momentum to the molecule, and the distance between the peaks in the high-end part of the spectrum decreases, resulting in their overlap. For $F \geqslant 2.8$ J/cm^2, the spectra are dominated by a single broad peak centered at approximately 22 GHz. Such clustering of spectral lines or band of equidistant states has no counterpart in the gas phase and has not been observed before for molecules in helium droplets.

---

[1]The $\langle \cos^2 \theta_{2D} \rangle$ traces were actually recorded out to 1200 ps. However, in order to exclude noise, the power spectra in Fig. 1 were computed using a Hamming window over only the signal bearing part of the $\langle \cos^2 \theta_{2D} \rangle$ traces. This window ranged from the full 1200-ps trace for the lowest fluences to the first 400 ps for the highest fluence.
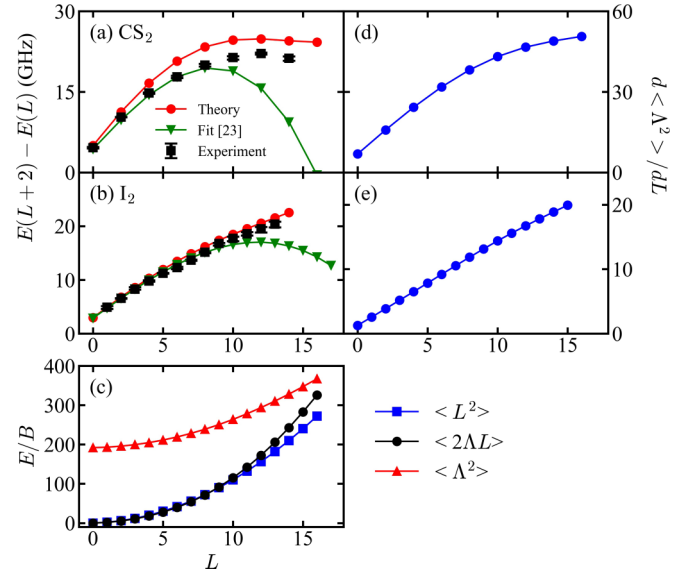

FIG. 2. (a) and (b) Frequency differences $(E_{L+2} - E_L)/h$ as a function of L for (a) CS$_2$ and (b) I$_2$. The black squares are the experimental results obtained from the central positions of the peaks in the spectra (cf. Fig. 1), the red circles are the results from the theoretical model, and the green triangles are the values from Eq. (1) using the data obtained in [23]. (c) The three contributions to the rotational energy of I$_2$ molecules in He droplets. (d) and (e) First derivative of the He solvent angular momentum squared $d\langle \mathbf{\Lambda}^2 \rangle/dL$ for (d) CS$_2$ and (e) I$_2$.

The series of spectra recorded at incrementally increasing F allows us to identify a total of eight peaks [24]. They reflect the frequencies of the $L \leftrightarrow L + 2$ coherences of the rotational wave packets [23], where L represents the total angular momentum. In Fig. 2(a) the peak positions, given by $(E_{L+2} - E_L)/h$ [23], are plotted as a function of $L = 0, 2, \ldots, 14$. Similarly, we identified 13 peaks in the spectra of I$_2$ [24]. Their central positions are plotted in Fig. 2(b). The details on identification of spectral lines are provided in [24].

For our theoretical model we start from general considerations that are dependent neither on the molecular species nor on the details of the molecule-solvent interactions. Considering only the addition of angular momenta, the rotational part of the Hamiltonian for a linear-rotor molecule in a solvent can be written as

$$\hat{H}_{\rm rot} = B\hat{\mathbf{J}}^2 = B(\hat{\mathbf{L}} - \hat{\mathbf{\Lambda}})^2. \quad (2)$$

Here B is the gas-phase rotational constant of the molecule, $\hat{\mathbf{J}}$ is the rotational angular momentum of the molecule, $\hat{\mathbf{\Lambda}}$ is the angular momentum carried by the surrounding solvent [28], and $\hat{\mathbf{L}}$ is the total angular momentum, which is the only conserved quantity in the presence of molecule-solvent interactions.

The Hamiltonian (2) can be mapped onto an effective symmetric-top Hamiltonian similar to that of linear open-shell molecules, such as OH or NO [29], with the solvent angular momentum $\hat{\mathbf{\Lambda}}$ playing the role of the electron angular momentum. The corresponding states can be expressed through the
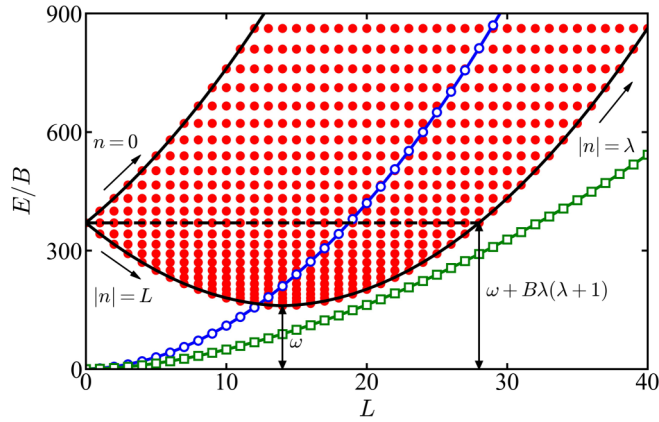
FIG. 3. The gas-phase molecular rotational states (blue open circles) are perturbed by a band of excited states (red closed circles; only single solvent excitations are shown), resulting in the rotational states of the molecule in the presence of the solvent (green open squares; a calculation for the I_2 molecule including multiple solvent excitations is shown).

symmetric top states $|LnM\rangle$, where n and M label the projection of $\hat{\mathbf{L}}$ on the molecular and laboratory axes, respectively.[2]

From Eq. (2) one can see that the energies corresponding to a given value of L depend on the value of $\mathbf{\Lambda}$. In other words, the rotational constant of a molecule in a solvent is, strictly speaking, not renormalized. Rather, the change of the rotational energies compared to the gas-phase case can be explained by the finite value of $\mathbf{\Lambda}$ (discussed below).

Let us assume that an excitation of the solvent has angular momentum λ and energy ω. While in the case of superfluid helium it might be tempting to label these excitations as rotons, we intentionally keep the treatment as general as possible and focus solely on energy and angular momentum conservation. If we initially include only single excitations of the solvent and consider only the diagonal terms in Eq. (2) in the $|LnM\rangle$ basis, the eigenvalues of $\hat{H}_{\text{rot}}$ are given by

$$E_{L,n} = BL(L+1) - 2Bn^2 + B\lambda(\lambda+1) + \omega, \quad (3)$$

where we introduced an additional energy shift by the excitation energy ω. Equation (3) corresponds to an oblate symmetric top shifted by $B\lambda(\lambda+1) + \omega$ from the zero energy, whose eigenstates are given by $|LnM\rangle$. When the off-diagonal terms of $\hat{H}_{\text{rot}}$ are taken into account, $|LnM\rangle$ states with different n's are mixed. This alters the eigenenergies compared to Eq. (3) and renders n an approximate quantum number. In what follows, we retain n to label the eigenenergies $E_{L,n}$.

The red closed circles in Fig. 3 show $E_{L,n}$ with off-diagonal terms of $\hat{H}_{\text{rot}}$ included. For each L (conserved quantity), the $E_{L,n}$'s form a band of $2n + 1$ excited states, originating at $B\lambda(\lambda+1) + \omega$. Due to molecule-solvent interactions, whose exact form is for now irrelevant, these states couple to the free molecular states $E_L^{(0)} = BL(L+1)$ (blue open circles). This perturbation results in the rotational states of the He-solvated molecules, shown by green open squares. Note that

these states were determined by taking into account single, double, and triple solvent excitations. Figure 3 shows, however, only states from single excitations to avoid an unreadable figure. The data presented in Fig. 3 were calculated for the I_2 molecule since it has both even and odd rotational states, but the qualitative features of the energy of the states are general.

The shape of the band of excited states is determined by the range of the possible projections $-L \leqslant n \leqslant L$ (for a linear molecule and single excitation, $|n| \leqslant \lambda$ must also be fulfilled). In the language of perturbation theory, the closer the band edge is to the blue line, the stronger the free molecular state perturbed by the solvent excitations is and the more the green squares deviate from the gas-phase behavior. The perturbation is the strongest after the free molecular states cross the excitation threshold at an energy of approximately ω, which happens for $L \gtrsim 12$ [cf. Fig. 2(c)].

Let us consider a linear rotor coupled to a bosonic bath with a single mode carrying energy ω and angular momentum λ, as described by the Hamiltonian in the molecular frame [28]

$$\hat{H} = B(\hat{\mathbf{L}} - \hat{\mathbf{\Lambda}})^2 + \omega \sum_\mu \hat{b}_{\lambda\mu}^\dagger \hat{b}_{\lambda\mu} + u(\hat{b}_{\lambda 0}^\dagger + \hat{b}_{\lambda 0}), \quad (4)$$

where u gives the molecule-solvent interaction strength and $\hat{b}_{\lambda\mu}^\dagger$ ($\hat{b}_{\lambda\mu}$) creates (annihilates) a solvent excitation with angular momentum λ and projection onto the molecular axis μ. We diagonalize the Hamiltonian in the basis containing multiple excitations of the single bosonic mode and all possible projections n,

$$\psi_{L[n_1 n_2 \cdots n_m],M}^{(m)} = |LNM\rangle_{\text{mol}} (b_{\lambda n_1}^\dagger b_{\lambda n_2}^\dagger \cdots b_{\lambda n_m}^\dagger |0\rangle_{\text{bos}}), \quad (5)$$

where $N = \sum n_i$ (with $|N| \leqslant L$) is the total angular momentum projection of the bosons. We take into account the states with $m \leqslant 3$; however, the arguments used for the single-excitation case of Fig. 3 above still hold in this case. Most importantly, the asymptotic behavior of the excited state band at $L \to \infty$ is identical to that shown in Fig. 3.

The introduced model is, on the one hand, a simplification of the original angulon model [28]. The Hamiltonian in Eq. (4) is obtained by replacing the continuous dispersion relation $\omega(k)$ with the single mode ω. On the other hand, we substantially expand the basis of wave functions. Including multiple excitations of the bosonic mode allows us to describe a broad range of molecules within the simple weak-coupling theory.

We used the model to calculate the rotational energies of CS_2 and I_2 molecules in He droplets (the values of the parameters are listed in [24]). Green squares in Fig. 3 represent the results for I_2. For comparison with experiment, the frequency differences $(E_{L+2} - E_L)/h$ were determined and plotted in Figs. 2(a) and 2(b) by red circles. For both I_2 and CS_2 there is good agreement between the experimental and theoretical results. Notably, the model predicts that the difference spectrum exhibits a maximum frequency around 20–25 GHz, which is very similar to that observed in experiment. Such a maximum never occurs for a free rotor where the position of a spectral line $(E_{L+2} - E_L)/h = 4L + 6$ increases linearly with L.[3]

---

[2]Note that for a linear molecule, n corresponds to the projection of $\hat{\mathbf{\Lambda}}$ on the molecular axis, since the projection of $\hat{\mathbf{J}}$ vanishes.

[3]Only at extreme values of L, reachable by an optical centrifuge, will centrifugal distortion cause a deviation from the linear behavior [30].
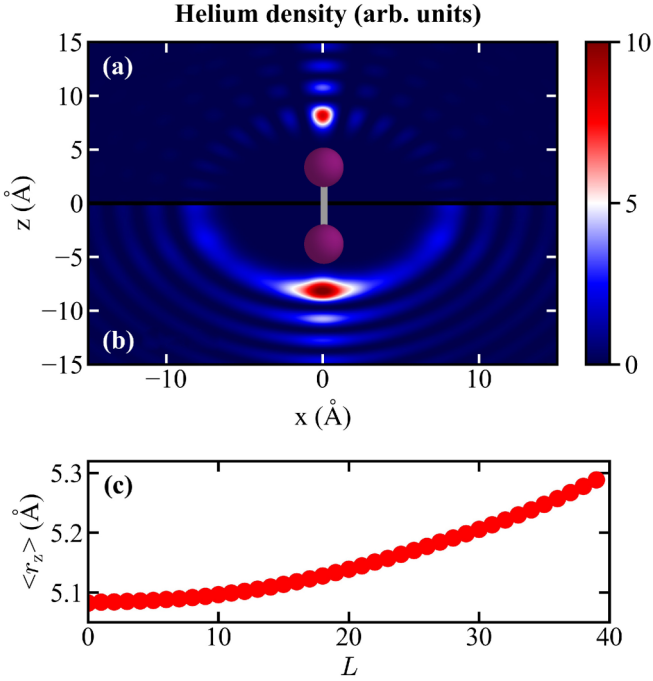
Helium density (arb. units)

FIG. 4. Anisotropic component of the helium density in the molecular frame for (a) $L = 0$ and (b) $L = 40$. (c) The average distance of He atoms from the molecular z axis grows with the angular momentum L. All plots are for the I_2 molecule.

In what follows, we show how the rotational energy structure of molecules in He droplets can be rationalized in terms of a single quantity, the angular momentum of the solvent $\mathbf{\Lambda}$. Figure 2(c) displays the L dependence of $B\langle \mathbf{L}^2 \rangle$, $B\langle \mathbf{\Lambda}^2 \rangle$ and $B\langle 2\mathbf{\Lambda} \cdot \mathbf{L} \rangle$, the three contributions to the molecular rotational energy [cf. Eq. (2)], calculated for I_2 molecules (the curves for CS_2 show a similar behavior [24]).

For $L = 0$, a nonrotating molecule is dressed by the excitations of the solvent due to molecule-He interactions. The corresponding many-particle state is given by a superposition of the basis states (5) with zero and nonzero angular momentum, which results in a nonzero expectation value $\langle \mathbf{\Lambda}^2 \rangle$ [see Fig. 2(c)]. Note that in order to have $\langle \mathbf{\Lambda}^2 \rangle \neq 0$, the solvent atoms do not need to be physically rotating. Barely placing an anisotropic molecule into the solvent deforms its density in a nonspherically symmetric fashion and thereby provides it with a nonzero angular momentum (cf. Fig. 4).

Figure 2(c) shows that $\langle \mathbf{L}^2 \rangle \approx \langle 2\mathbf{\Lambda} \cdot \mathbf{L} \rangle$ up to $L \sim 10$, which implies that $\langle \mathbf{J}^2 \rangle = \langle (\mathbf{L} - \mathbf{\Lambda})^2 \rangle \approx \langle \mathbf{\Lambda}^2 \rangle$, i.e., the angular momenta of the solvent and of the molecule are equal to each other. Classically, this can be understood as follows. At small values of L, the He atoms are almost rigidly attached to the molecule and corotate with the molecule, which results in the equal magnitude of the molecular and solvent angular momenta. This is analogous to the nonsuperfluid solvation shell, previously discussed in the literature [25]. In order for the molecular rotation to be able to perturb the solvation shell, the rotational kinetic energy must be comparable to the energy of the solvent excitations, i.e., $BL(L + 1) \sim \omega$, which for I_2 molecules corresponds to $L \sim 12$. Around this point we observe the deviations of $\langle 2\mathbf{\Lambda} \cdot \mathbf{L} \rangle$ from $\langle \mathbf{L}^2 \rangle$ in Fig. 2(c).

As we show in Figs. 2(d) and 2(e), the derivative of $d\langle \mathbf{\Lambda}^2 \rangle/dL$ alone is able to describe the experimental data on the rotational energy splittings [Figs. 2(a) and 2(b)] quite accurately. From this plot one can clearly see the origin of the renormalized spectroscopic constants of Eq. (1). The linear behavior of $d\langle \mathbf{\Lambda}^2 \rangle/dL$ corresponds to an effective B^*. The deviations of $d\langle \mathbf{\Lambda}^2 \rangle/dL$ from the linear behavior, together with the contributions from the $\langle 2\mathbf{\Lambda} \cdot \mathbf{L} \rangle$ at higher L, lead to higher-order terms such as $D^*L^2(L + 1)^2$. Furthermore, while the magnitude of $\langle \mathbf{\Lambda} \rangle$ grows with L, it saturates and assumes a constant value for large L [24]. As a result, Λ plays a decreasing role for $L \to \infty$, meaning that the rotational spectrum eventually approaches that of the gas phase, which can classically be interpreted as detachment of the molecule from the surrounding superfluid [31].

Moreover, the model yields analytic expressions for B^* and D^* in agreement with experiments [25]. In the basis of single solvent excitations, the constants can be approximated as [24]

$$\frac{B^*}{B} \approx 1 - \frac{\tilde{u}^2}{(1 + \tilde{\omega})^3}, \quad \frac{D^*}{B} \approx \frac{\tilde{u}^2}{\lambda(\lambda + 1)(1 + \tilde{\omega})^5}, \quad (6)$$

with $\tilde{u} = u/[B\lambda(\lambda + 1)]$ and $\tilde{\omega} = \omega/[B\lambda(\lambda + 1)]$. In the limit of light molecules $(\tilde{u}, \tilde{\omega}) \to 0$, B^* approaches B. Furthermore, Eq. (6) provides a useful relation $D^*/B \approx \xi(1 - B^*/B)^{5/3}$, with $\xi = \tilde{u}^{-4/3}/[\lambda(\lambda + 1)]$. This dependence is similar to the power law $D^* = 0.031 \times B^{*1.818}$ found in Ref. [13], but provides a correct limit of $D^* \to 0$ for $B^* \to B$.

To illustrate what the change of angular momentum of Fig. 2(c) corresponds to in real space, we used the model to evaluate the helium density distribution in the molecular frame, as shown in Figs. 4(a) and 4(b) for $L = 0$ and 40, respectively. Note that since our model accounts for He droplet excitations by a single mode only and does not take into account a full molecule-He potential energy surface, the model is not expected to provide quantitatively accurate density estimates. We observe that with the growth of L, the solvent atoms slightly move from the direction parallel to the molecular axis (linear configuration) towards the T-shape configuration, which is clearly visible in the average distance of the He atoms from the z axis [Fig. 4(c)]. This reflects the fact that the B^* and D^* constants can be interpreted in terms of formation of the molecule–He-shell complex and the displacement of the He atoms due to rotation of the complex.

In conclusion, through picosecond time-resolved alignment experiments, we measured the rotational energy levels of CS_2 and I_2 in He droplets up to $L = 16$ and 15, respectively. The results agree well with the outcome of a quantum model, which also shows that the rotational energy structure can be understood in terms of the angular momentum transferred from the molecules to the He solvent. Interesting future challenges for both experiments and theory include an understanding of the lifetimes of the highest excited states observed.

[1] K. Nauta and R. E. Miller, J. Chem. Phys. **115**, 10254 (2001).

[2] S. Grebenev, M. Hartmann, M. Havenith, B. Sartakov, J. P. Toennies, and A. F. Vilesov, J. Chem. Phys. **112**, 4485 (2000).

[3] K. Nauta and R. E. Miller, J. Chem. Phys. **115**, 8384 (2001).

[4] M. Hartmann, R. E. Miller, J. P. Toennies, and A. Vilesov, Phys. Rev. Lett. **75**, 1566 (1995).

[5] E. Lee, D. Farrelly, and K. B. Whaley, Phys. Rev. Lett. **83**, 3812 (1999).

[6] Y. Kwon and K. B. Whaley, Phys. Rev. Lett. **83**, 4108 (1999).

[7] C. Callegari, A. Conjusteau, I. Reinhard, K. K. Lehmann, G. Scoles, and F. Dalfovo, Phys. Rev. Lett. **83**, 5058 (1999).

[8] K. K. Lehmann, J. Chem. Phys. **114**, 4643 (2001).

[9] K. K. Lehmann, J. Chem. Phys. **117**, 1595 (2002).

[10] R. E. Zillich, Y. Kwon, and K. B. Whaley, Phys. Rev. Lett. **93**, 250401 (2004).

[11] R. E. Zillich and K. B. Whaley, Phys. Rev. B **69**, 104517 (2004).

[12] M. Lemeshko, Phys. Rev. Lett. **118**, 095301 (2017).

[13] M. Y. Choi, G. E. Douberly, T. M. Falconer, W. K. Lewis, C. M. Lindsay, J. M. Merritt, P. L. Stiles, and R. E. Miller, Int. Rev. Phys. Chem. **25**, 15 (2006).

[14] I. Reinhard, C. Callegari, A. Conjusteau, K. K. Lehmann, and G. Scoles, Phys. Rev. Lett. **82**, 5036 (1999).

[15] C. Callegari, I. Reinhard, K. K. Lehmann, G. Scoles, K. Nauta, and R. E. Miller, J. Chem. Phys. **113**, 4636 (2000).

[16] R. Lehnig, P. L. Raston, and W. Jäger, Faraday Discuss. **142**, 297 (2009).

[17] H. Stapelfeldt and T. Seideman, Rev. Mod. Phys. **75**, 543 (2003).

[18] S. Fleischer, Y. Khodorkovsky, E. Gershnabel, Y. Prior, and I. S. Averbukh, Isr. J. Chem. **52**, 414 (2012).

[19] P. M. Felker, J. Phys. Chem. **96**, 7844 (1992).

[20] C. Riehn, Chem. Phys. **283**, 297 (2002).

[21] C. Schroter, K. Kosma, and T. Schultz, Science **333**, 1011 (2011).

[22] A. S. Chatterley, M. O. Baatrup, C. A. Schouder, and H. Stapelfeldt, Phys. Chem. Chem. Phys. **22**, 3245 (2020).

[23] A. S. Chatterley, L. Christiansen, C. A. Schouder, A. V. Jørgensen, B. Shepperson, I. N. Cherepanov, G. Bighin, R. E. Zillich, M. Lemeshko, and H. Stapelfeldt, Phys. Rev. Lett. **125**, 013001 (2020).

[24] See Supplemental Material at http://link.aps.org/supplemental/10.1103/PhysRevA.104.L061303 for details.

[25] J. P. Toennies and A. F. Vilesov, Ang. Chem. Int. Ed. **43**, 2622 (2004).

[26] B. Shepperson, A. S. Chatterley, A. A. Søndergaard, L. Christiansen, M. Lemeshko, and H. Stapelfeldt, J. Chem. Phys. **147**, 013946 (2017).

[27] A. A. Søndergaard, B. Shepperson, and H. Stapelfeldt, J. Chem. Phys. **147**, 013905 (2017).

[28] R. Schmidt and M. Lemeshko, Phys. Rev. X **6**, 011012 (2016).

[29] H. Lefebvre-Brion and R. W. Field, *The Spectra and Dynamics of Diatomic Molecules* (Elsevier, New York, 2004).

[30] A. A. Milner, A. Korobenko, J. W. Hepburn, and V. Milner, J. Chem. Phys. **147**, 124202 (2017).

[31] B. Shepperson, A. A. Søndergaard, L. Christiansen, J. Kaczmarczyk, R. E. Zillich, M. Lemeshko, and H. Stapelfeldt, Phys. Rev. Lett. **118**, 203203 (2017).